Vapor−Liquid and Vapor−Solid Phase Equilibria for United-Atom Benzene Models near Their Triple Points: The Importance of Quadrupolar Interactions

Xin S. Zhao,[†] Bin Chen,[‡] Sami Karaborni,[§] and J. Ilja Siepmann*[,†]

Departments of Chemistry and of Chemical Engineering and Material Science, University of Minnesota, 207 Pleasant Street SE, Minneapolis, Minnesota 55455-0431, Department of Chemistry, Louisiana State University, 232 Choppin Hall, Baton Rouge, Louisiana 70803-1804, and Pharmaceutical Research & Development, Merck & Company Inc., P.O. Box 4, WP78-304, West Point, Pennsylvania 19486

Received: August 13, 2004; In Final Form: January 7, 2005

Gibbs ensemble Monte Carlo simulations were used to calculate the vapor−liquid and vapor−solid coexistence curves for benzene using two simple united-atom models. An extension of the Gibbs ensemble method that makes use of an elongated box containing a slab of the condensed phase with a vapor phase along one axis was employed for the simulations of the vapor−solid equilibria and the vapor−liquid equilibria at very low reduced temperatures. Configurational-bias and aggregation-volume-bias Monte Carlo techniques were applied to improve the sampling of particle transfers between the two simulation boxes and between the vapor and condensed-phase regions of the elongated box. An isotropic united-atom representation with six Lennard-Jones sites at the positions of the carbon atoms was used for both force fields, but one model contained three additional out-of-plane partial charge sites to explicitly represent benzene's quadrupolar interactions. Both models were fitted to reproduce the critical temperature and density of benzene and yield a fair representation of the vapor−liquid coexistence curve. In contrast, differences between the models are very large for the vapor−solid coexistence curve. In particular, the lack of explicit quadrupolar interactions for the 6-site model greatly reduces the energetic differences between liquid and solid phases, and this model yields a triple point temperature that is about a factor of 2 too low. In contrast, the 9-site model predicts a triple point of benzene at $T = 253 \pm 6$ K and $p = 2.3 \pm 0.8$ kPa in satisfactory agreement with the experimental data ($T = 278.7$ K and $p = 4.785$ kPa).

I. Introduction

Benzene is the prototypical aromatic hydrocarbon and for a long time has been one of the most important solvents and chemical feedstocks for many processes. Thus, there is great interest to find molecular models that yield a good description of the thermophysical properties of benzene.[1−12] Models used for benzene include, for example, highly simplified 6-site Lennard-Jones models with or without central quadrupole, 6-site models with distributed multipoles and anisotropic repulsive interactions, or polarizable 12-site models. Most of these models were developed to reproduce selected properties of either the solid or the liquid phase. With the exception of the anisotropic 6-site model proposed by Yashonath et al.,[5] the other models have either not been tested or failed to yield good agreement for the liquid and the two solid phases, that is a low-temperature, low-pressure orthorhombic phase, space group *Pbca*,[13,14] and a high-pressure monoclinic phase, space group $P2_1/c$.[15] More recently, the ability of different force fields and computational search procedures to reproduce the polymorphic nature of benzene has been investigated,[16−23] and an excellent comparison of these attempts has been published.[23] Nevertheless, to the knowledge of these authors, only Schroer and Monson have reported on particle-based simulation studies for the solid−fluid phase equilibria of benzene.[24,25] Schroer and Monson employed the free energy method of Frenkel and Ladd[26,27] and used a 6-site hard sphere representation to model the shape of benzene with a range of values for the quadrupole moment. They concluded that the quadrupolar interaction is essential to stabilize benzene I and that a model with a quadrupole moment close to benzene's gas-phase value yields a volume change upon freezing that is in good agreement with the experimental value for benzene.[25] In addition, Schroer and Monson also found that a combination of perturbation theory for the fluid phase[28] and cell theory for the solid phase[29] yields good agreement with their particle-based simulations.

The present paper builds on the work of Schroer and Monson by using similar 6-site models without and with an explicit quadrupole, but replacing the hard-sphere site−site potential by the Lennard-Jones 12-6 potential[30] with the well depth and size parameters adjusted to reproduce the vapor−liquid coexistence envelope of benzene.[11,12] Thus, the present simulations allow for a direct comparison with the experimentally observed phase behavior of benzene. In contrast to a thermodynamic integration procedure,[26] direct calculations of the vapor−liquid and vapor−solid coexistence curves were performed for this work using a recent extension[31] of the Gibbs ensemble Monte Carlo (GEMC) method.[32,33] The triple point temperature can then be determined from the intersection of the two coexistence lines in a Clausius−Clapeyron plot.[31]

The next section gives a brief description of the two benzene models and the simulation details. The results of the GEMC simulations are presented and extensively discussed in section III, followed by some concluding remarks.

* Address correspondence to this author. E-mail: siepmann@chem.umn.edu.
[†] University of Minnesota.
[‡] Louisiana State University.
[§] Merck & Company Inc.

10.1021/jp046339f CCC: $30.25
Published on Web 02/24/2005

TABLE 1: TraPPE Force Field Parameters for United-Atom Benzene Models

	σ [Å]	ϵ/k_B [K]	bond length [Å]	Θ [10^{-40} C m^2]
6-site[a]	3.695	50.5	1.40	0
9-site[b]	3.740	48.0	1.40	−23.9

[a] Reference 11. [b] Reference 12.

II. Models and Simulation Details

A. Benzene Models. In this work, the 6-site and 9-site united-atom representations for benzene were taken from the transferable potentials for phase equilibria (TraPPE) force field.[11,12] In these models the repulsive and dispersive interactions are modeled by six CH pseudoatoms placed at the position of the carbon nuclei of a rigid hexagon with a bond length of 1.40 Å. The intermolecular site−site interactions are described by a pairwise additive Lennard-Jones (LJ) 12-6 potential and, for the 9-site model, Coulombic interactions of three partial charges

$$U_{LJ}(r_{ij}) = 4\epsilon\left[\left(\frac{\sigma}{r_{ij}}\right)^{12} - \left(\frac{\sigma}{r_{ij}}\right)^{6}\right] + \frac{q_i q_j}{4\pi\epsilon_0 r_{ij}} \qquad (1)$$

where r_{ij}, ϵ, σ, q_i and q_j, and ϵ_0 are the bead−bead separation, the LJ well depth, the LJ diameter, partial charges, and permittivity of vacuum, respectively. The LJ parameters were determined by a fit to the critical temperature and the saturated liquid density at near ambient conditions and are listed in Table 1. Although the 6-site model yields an adequate reproduction of the vapor−liquid coexistence curve for neat benzene (e.g., the normal boiling point is underestimated by about 12 K), the neglect of explicit quadrupole interactions requires a compensation by an increase of the LJ well depth which, in turn, leads to an overestimation of the strength of the interactions with nonpolar molecules, such as normal alkanes, and a corresponding underestimation of the separation factors.[11] As a remedy, a 9-site model was later developed[12] that for consistency with other polar molecules uses three extra partial charge sites to represent the quadrupole moment. These charge sites are located symmetrically on the 6-fold axis with a positive charge of +2.42 e placed in the benzene plane and two compensating negative partial charges at a distance of 0.785 Å[34] representing the π-electron clouds on both sides. The quadrupole moment of this 9-site model is -23.9×10^{-40} C m^2, which is within the range of the values measured experimentally.[35] Use of the 9-site model results in a slight lowering of the saturated vapor pressure and a corresponding increase of the normal boiling point (that is too low by only 6 K), but its major benefit compared to the 6-site model is the greatly improved description for alkane−arene interactions that allowed for accurate prediction of separation factors and the temperature dependence of relative retention times in gas−liquid chromatography for these molecules.[12]

There is a relatively wide range of LJ parameters used for CH pseudoatoms proposed by other researchers (e.g., $\sigma = 3.50$ Å and $\epsilon/k_B = 77.0$ K for the model by Evans and Watts,[1] 3.72 Å and 55.3 K by Claessens et al.,[2] and $\sigma = 3.75$ Å and $\epsilon/k_B = 55.4$ K by Jorgensen et al.[3]), and the values determined for the 6- and 9-site TraPPE-UA models lie at the upper end of the range for the LJ diameter and somewhat below this range for the well depth.

B. Simulation Details. Two series of GEMC simulations were carried out to determine the vapor−liquid and vapor−solid coexistence curves near the triple point for both the 6-site and the 9-site TraPPE-UA models. The conventional Gibbs ensemble setup with two cubic simulation cells[32,33] was used for most simulations of vapor−liquid equilibria ($N = 800$), and the solid-slab GEMC method[31] was applied to vapor−solid equilibria. The solid slab simulations were started from a configuration based on the experimentally determined structure of benzene I that is stable at low pressures.[13] In particular, the solid slab consisted of $5 \times 5 \times 8$ unit cells ($N = 800$) with the lattice constants of $a = 7.460$ Å, $b = 7.034$ Å, and $c = 9.666$ Å and was placed in a periodically replicated simulation box of dimensions 37.30 Å × 35.17 Å × 160 Å. Thus, the solid material was surrounded by vapor on both sides in the *z*-direction and had no interface in either *x*- or *y*-directions. A separate cubic box was used for the vapor phase and allows for a more precise determination of the saturated sublimation pressure.[31] The volume of the vapor box was adjusted depending on the model and the simulation temperature to yield vapor phases with between 40 and 200 molecules to allow for a reliable determination of the saturation pressure.

In some of the solid-slab GEMC simulations for the 6-site benzene model (that yields a far too low triple point temperature, see below), the entire slab melted and the saturated vaporization pressure was directly estimated from these simulations now containing a liquid slab. Additional conventional GEMC simulations were carried out at some of these temperatures to verify that the liquid slab and fully periodic bulk liquid yield the same properties.

Since the solid-slab approach does not allow for a straightforward calculation of the tail corrections for the LJ potential, we opted to use a spherical truncation at 16 Å based on the distance of individual pseudoatoms for the LJ interactions and based on the center-of-mass distance of two molecules for the Coulombic interactions. Using a spherical truncation for *both* LJ and Coulombic interactions is advantageous (at least for weakly polar systems) because the effects of the two truncation errors do partially cancel each other. The LJ tail corrections are always attractive (i.e., increase the magnitude of the cohesive energy and lower the saturated vapor pressure), whereas the Ewald summation technique for periodic systems usually results in a net repulsion. This cancellation of truncation errors is evident from the good agreement obtained for the vapor−liquid coexistence curves of benzene computed with simple spherical truncation and with tail correction and Ewald sum (see below). A similar observation was made previously for the phase diagram of carbon dioxide.[31]

Five different types of moves were employed in all GEMC simulations including center-of-mass translations, rotations around the center of mass, volume exchanges between the two simulation boxes (where these moves used separate displacements of the individual cell parameters for the solid-slab simulations[36]), particle swap moves using configurational-bias strategies,[37−41] and aggregation-volume-bias Monte Carlo moves[42,43] for solid-to-vapor and vice versa transfer moves in the solid-slab box. It should be mentioned here that the particle swap moves used in the present simulations sample space uniformly in the solid-slab Gibbs ensemble, i.e., the location of insertion sites is not biased by knowledge of the slab location nor is any attempt made to preferentially remove particles from specific regions of the solid slab. However, aggregation-volume-bias techniques[42,43] could be used to bias particle swaps to the surface region.

For every temperature, the simulations were equilibrated for at least 200 000 Monte Carlo cycles (one cycle consists of $N = 800$ randomly selected trial moves), and the production periods ranged from 200 000 to 1 000 000 cycles. The solid-slab GEMC simulations were carried out following a two-step procedure. First, relatively short solid-slab simulations were carried out to

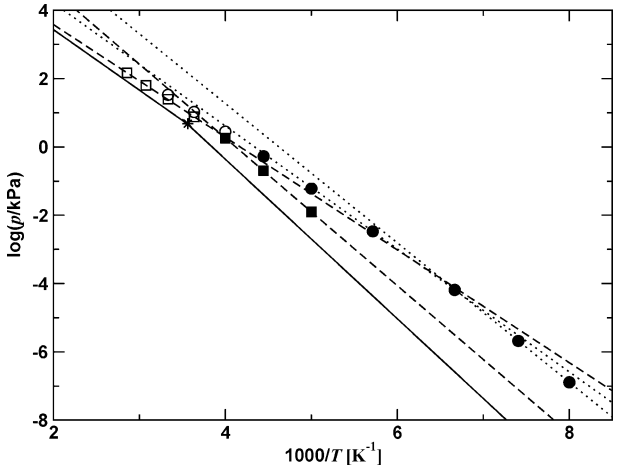

Figure 1. Clausius−Clapeyron plots of the sublimation and vaporization pressure curves versus the inverse temperature. The solid lines depict the experimental data.[45,46] The star is the intersection of the two solid lines and indicates the experimental triple point. The circles and squares show simulation results for the 6-site and 9-site models, respectively. The filled and open symbols represent the data from Gibbs ensemble simulations using the slab and the conventional setup, respectively. The dotted and dashed lines depict weighted-linear least-squares fits to the sublimation and vaporization pressure data for the 6-site and 9-site models, respectively.

obtain a rough estimate of the triple point location. This was followed by a full simulation (of the length mentioned above) at a temperature lying a few percent below the rough estimate of the triple point temperature. If the solid slab remained stable throughout this long simulation, then its heat of sublimation was computed and used to determine appropriate conditions (size of the vapor box) for the next lower temperature. Thereby, this iterative procedure makes use of the advantages of the Gibbs−Duhem integration approach.[44]

III. Results and Discussion

A. Phase Equilibria. The pressure−inverse temperature phase diagrams calculated using both benzene models are compared to the experimental data[45,46] in Figure 1. The calculated sublimation and vaporization pressures for both models can be well fit by straight lines as prescribed by the Clausius−Clapeyron (CC) equation.[47] The triple point can be determined from the extrapolated intersection of these two lines. It should be noted here that when the solid-slab Gibbs ensemble simulations were extended above the triple point temperature, one could observe surface-induced melting, thus the presence of the interface prevents the sampling of a superheated solid phase and an upper bound for the triple point temperature is easily established. For example, the slab simulation at $T = 150$ K for the 6-site model yielded a liquid phase despite that the temperature is only a few degrees Kelvin above the extrapolated triple point temperature.

The thermodynamic properties of both benzene models at their triple points are summarized in Table 2. The triple-point locations determined from the CC fits for the 6-site and 9-site models are $p = (5 \pm 4) \times 10^{-5}$ kPa at $T = 148 \pm 6$ K and $p = 2.3 \pm 0.8$ kPa at $T = 253 \pm 6$ K, respectively. The triple point pressure and temperature for the 6-site model are far below the experimental values of 4.785 kPa at 278.7 K.[48] In contrast, the triple point temperature of the 9-site model is only 10% below the experimental value and the triple point pressure for the 9-site model is too low by a factor of about two. The ratios of the triple point over critical point parameters calculated for both TraPPE models and measured experimentally are also listed in Table 2. Again, agreement for the 9-site model with experiment is fair with a reduced triple point temperature similar to that for Lennard-Jonesium[31,49] but well below the value for carbon dioxide, another example of a small quadrupolar molecule.[31] In contrast, the reduced triple point temperature for the 6-site model is far too low and yields a value similar to propane,[50] i.e., at the lower end of the range for small molecules. Thus, as also found by Schroer and Monson,[25] the inclusion of an explicit quadrupole moment yields a dramatic stabilization of the benzene I solid phase compared to a model without a quadrupole moment.

The heats of sublimation and vaporization calculated directly from the Gibbs ensemble simulations[51] and obtained from the CC fits are shown in Figure 2. Since the statistical uncertainties in both the saturated sublimation pressure and density are relatively large at low reduced temperatures, the statistical errors in the enthalpies of sublimation are quite large. The heats of vaporization and sublimation for both the 6-site and 9-site models fall below the range of the experimental values[52,53] with the deviation for the 6-site model being somewhat larger. Most important, the heat of fusion at the triple point appears to be greatly underestimated by the 6-site model, whereas the value for the 9-site model falls only slightly below the experimental value.

The temperature−density phase diagrams for both models are shown in Figure 3. The vapor−liquid coexistence data at elevated temperatures (above 350 K) were taken directly from the original work by Wick et al.[11,12] and are based on simulations using a shorter value of 14 Å for the spherical potential truncation but with tail corrections for the Lennard-Jones part and Ewald summation for the long-range Coulombic interactions of the 9-site model. As mentioned above, a cutoff at 16 Å for both Lennard-Jones and Coulombic interactions without long-range corrections was used in this work. However, the effect of this change on the temperature−density curve (and also the saturated vapor pressures) is rather small. The saturated liquid densities for both models are in good agreement with experiment over the entire liquid range from experimental triple point to critical point. In contrast, the saturated solid densities are underpredicted by about 2% for the 9-site model at $T = 250$ K and 5% the 6-site model at $T = 145$ K. As can be seen from Figure 3 and the numerical data in Table 2, the 9-site model yields a liquid-to-solid density jump at the triple point of about 11% in fair agreement with the experimental value of 14%, whereas the corresponding jump for the 6-site model is only 3%, i.e., explicit inclusion of quadrupolar interactions is essential to reproduce the density jump in agreement with the earlier simulations by Schroer and Monson.[25]

B. Structural Analysis. Snapshots of the final configurations and density profiles taken from the slab simulations for the 9-site model at three different temperatures (200, 250, and 275 K) are shown in Figures 4 and 5. When the temperature is well below the triple point temperature ($T = 200$ K), the entire slab remains in a well-ordered solid structure. The outermost layer shows a significant decrease in the peak height of the density profiles that can be partially attributed to minor translational disorder (a widening of the peak) and the appearance of a few surface defects. As the temperature approaches the triple point from below ($T = 250$ K), the peaks for the solid layers become less pronounced and surface-induced melting occurs in the outermost layers. There is significant positional disorder in what originally has been the outermost layer and some molecules are observed to form an additional layer. Above the triple point

TABLE 2: Thermodynamic Properties of Benzene at Its Triple Point (TP) and Vapor−Liquid (VL) and Vapor−Solid (VS) Coexistence Data Near the Triple Point[a]

		T [K]	p [kPa]	ρ_{sol} [g/mL]	ρ_{liq} [g/mL]	ρ_{vap} [mg/mL]	T_{trip}/T_{crit}	p_{trip}/p_{crit}
experiment[b]	TP	278.7	4.785	1.023^{c}	0.896	0.162	0.496	9.8×10^{-4}
6-site	TP	148_6	$5_4 \times 10^{-5}$	1.05_1	1.02_1	$1.9_{1.2} \times 10^{-6}$	0.26	10^{-8}
6-site	VL	150	$6.5_5 \times 10^{-5}$		1.018_1	$4.1_3 \times 10^{-6}$		
6-site	VS	135	$2.1_6 \times 10^{-5}$	1.060_1		$1.4_4 \times 10^{-6}$		
9-site	TP	253_6	2.3_8	1.01_2	0.91_2	0.07_3	0.45	5×10^{-4}
9-site	VL	275	6.7_4		0.886_2	0.26_2		
9-site	VS	250	1.7_3	1.013_3	−	0.06_1		

[a] Subscripts denote the statistical uncertainties in the last digits. [b] Reference 48. [c] At $T = 270$ K.

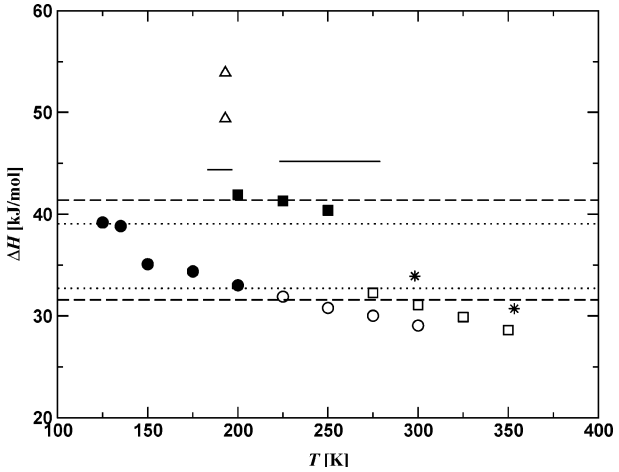

Figure 2. Heats of sublimation and vaporization as a function of temperature. Stars,[56] triangles,[52] and the solid lines[57] depict experimental data. Symbols denote the enthalpies calculated directly from the Gibbs ensemble simulations with symbol styles as in Figure 1. The dotted and dashed line depict the Clausius−Clapeyron fits for the 6-site and 9-site models, respectively.

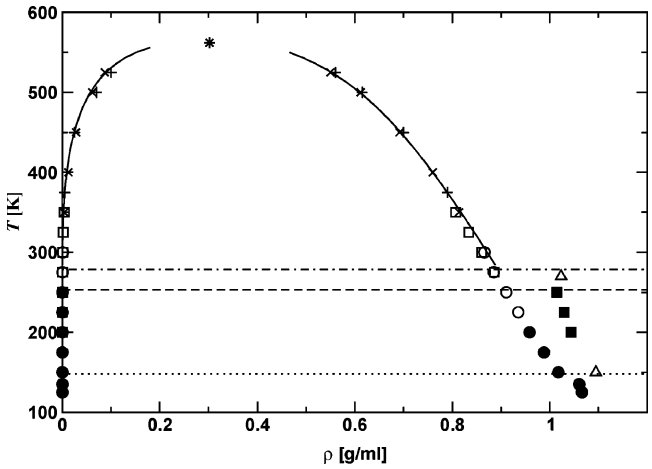

Figure 3. Vapor−liquid and vapor−solid coexistence curves for benzene. The solid lines, star, and triangles denote the experimental data for the vapor−liquid coexistence curve,[45] the critical point,[48] and low-temperature specific densities.[13] Filled and open circles and squares are used as in Figure 1. The plusses and crosses denote the high-temperature saturated densities for the 6-site and 9-site models, respectively, using a slightly different simulation protocol (see text). The horizontal dash−dotted, dotted, and dashed lines depict the triple point temperatures measured experimentally[45] and extrapolated from Clausius−Clapeyron fits for the 6-site and 9-site models, respectively.

($T = 275$ K), the entire slab has melted into a liquid film with a uniform density in its central part (see Figure 5). The same behavior upon increasing temperature was observed for the 6-site model, but shifted to much lower temperatures.

The crystal structure of benzene I belongs to the *Pbca* space group with the center of mass positions forming a face centered

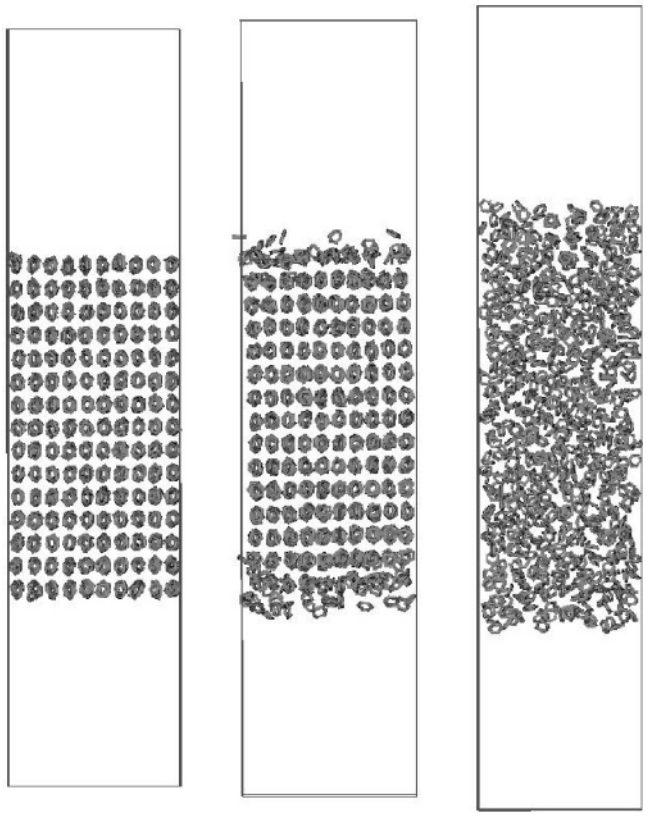

Figure 4. Snapshots depicting the final configurations of the slab simulations for the 9-site model $T = 200$ (left), 250 (middle), and 275 K (right). Projections onto the *xz*-plane are shown. The benzene rings are illustrated in stick representation.

orthorhombic structure. The planes of the benzene molecules are arranged in an approximate T-shaped pattern. Figure 6 shows the unit cell of benzene I and the definition of the angles θ and ϕ that are used for the subsequent analysis. An orientational order parameter S can be defined as follows:

$$S = \frac{1}{2}(3\cos^2\theta - 1) \qquad (2)$$

where θ is the azimuthal angle of a vector perpendicular to the benzene plane with the [001] axis. The orientational order parameter S takes a value of -0.5 if the reference vectors are perpendicular, a value of 1 if the reference vectors are parallel, and a value close to 0 for random orientations. The average orientational order parameters for the 6-site and 9-site models are plotted as function of *z*-position in Figure 7. Although the two models yield very similar order parameters for the interior part of the slab at the lowest temperature studied here ($T = 125$ and 200 K for the 6-site and 9-site models, respectively), there are striking differences in orientational order at the solid−vapor interface and in the temperature dependence

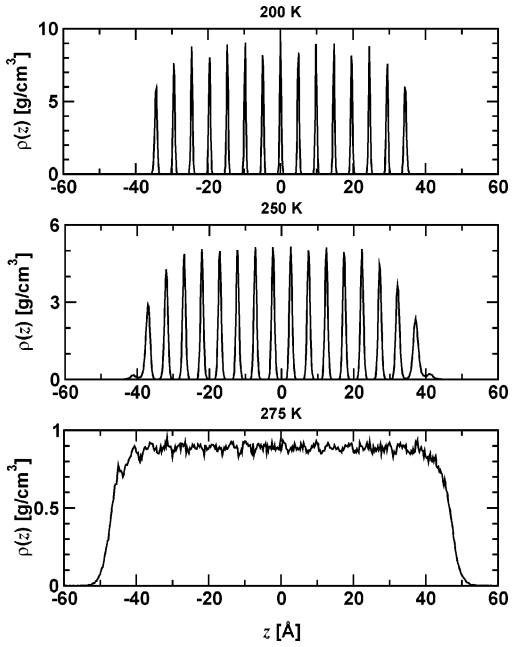

Figure 5. Center-of-mass density profiles as a function of position along the *z*-axis calculated from slab simulations for the 9-site model using a bin width of 0.2 Å. Results are shown for $T = 200$ (top), 250 (middle), and 275 K (bottom).

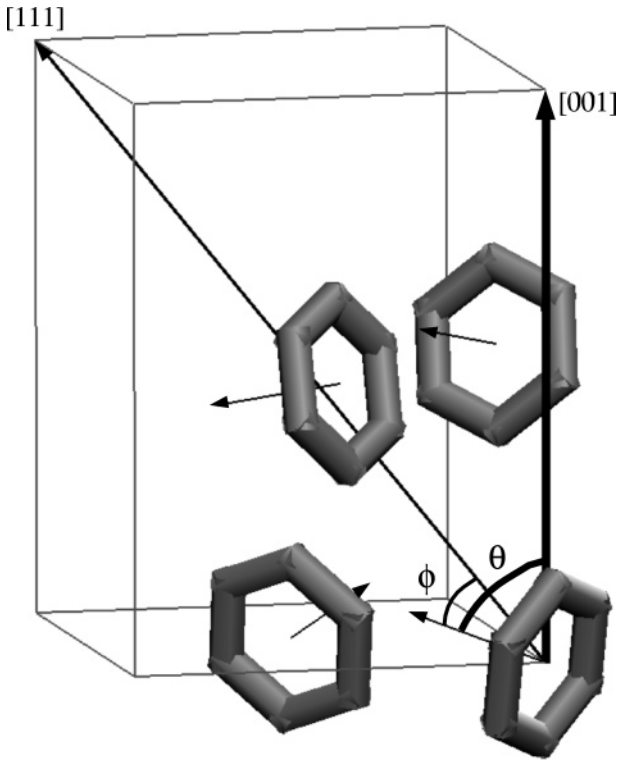

Figure 6. Unit cell of benzene I showing the orientation of the molecules and the definition of the angles θ and ϕ.

of the orientational order parameter. Even at the lowest temperature, there is significant orientational disorder observed for the surface layer of the 6-site model, whereas the surface layer for the 9-site model remains well ordered. This difference is accentuated as the temperature approaches the respective triple point values. At $T = 135$ K (about 10% below the estimated triple point temperature), the outermost three layers of the slab for the 6-site model show significant disorder. In contrast, the central part of the slab for the 9-site model remains

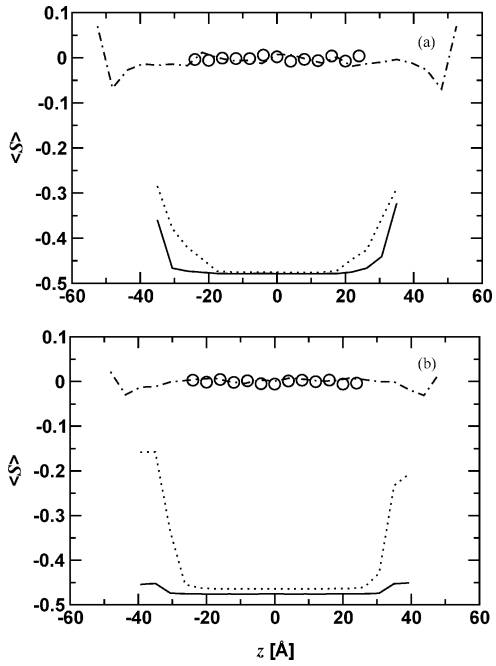

Figure 7. Averages of the orientational order parameter, *S*, as a function of position along the *z*-axis for the 6-site model (top) and the 9-site model (bottom). Solid, dotted, and dot−dashed lines and circles denote results obtained at the following temperatures (values for 9-site model in parentheses): 125 (200), 135 (250), 200 (275), and 300 K (350 K), respectively.

highly ordered even at $T = 250$ K (less than 2% below the estimated triple point temperature) and only the outermost two layers show significant disorder. Thus, it appears that explicit inclusion of the quadrupole moment dramatically alters the order at the surface and greatly reduces the onset of surface melting.

Further information on the orientational order can be obtained from the distribution of the azimuthal angle, ϕ, between the molecule plane vector and the [111] axis (see Figure 8). It should be noted that only the central part of the slab is used for this analysis.[51] There are two preferred orientations for ϕ that lead to a distribution with two peaks of about equal population. The distributions of ϕ show similar behavior for the two models (but offset in temperature) with a gradual decline of the peak heights as the triple point is approached and a uniform distribution for the liquid.

The distributions of the mutual orientation, ψ, between the planes of neighboring benzene molecules (up to a center-of-mass separation of 5.5 Å, the position of the first minimum of the center-of-mass radial distribution function) for the two models are shown in Figure 9. Again, the two models follow similar behavior as the temperature is raised. At similar relative temperatures below the triple point, however, the 9-site model yields a higher and narrower peak for the T-shaped arrangement that is stabilized by the explicit quadrupolar interactions. Furthermore, the solid phases for the 6-site model contain a very small fraction of defects where neighboring molecules are packed with parallel orientation. The distribution of mutual orientations in the liquid phase is nearly uniform for both models. However, a weak preference for parallel orientations (allowing more efficient packing) is evident for the liquid phase of the 6-site model. In contrast, the 9-site model shows very minor preferences for either parallel or perpendicular orientations (allowing for favorable quadrupolar interactions).

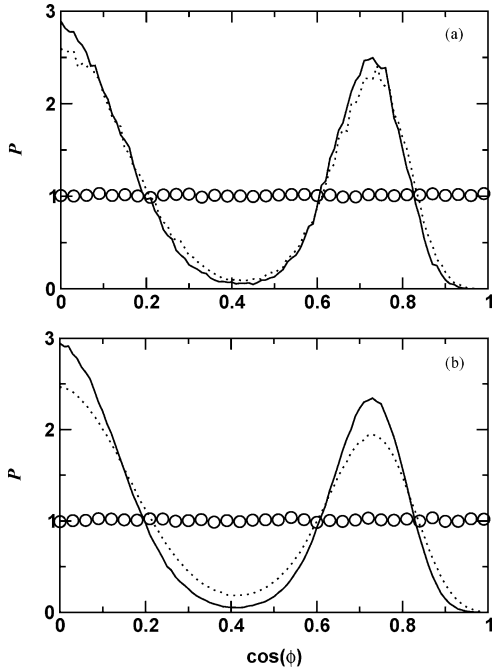

Figure 8. Distributions of the azimuthal angle ϕ with the [111] axis in the central region of the slab or the bulk liquid for the 6-site benzene model (top) and 9-site benzene model (bottom). Line styles and symbols as in Figure 7.

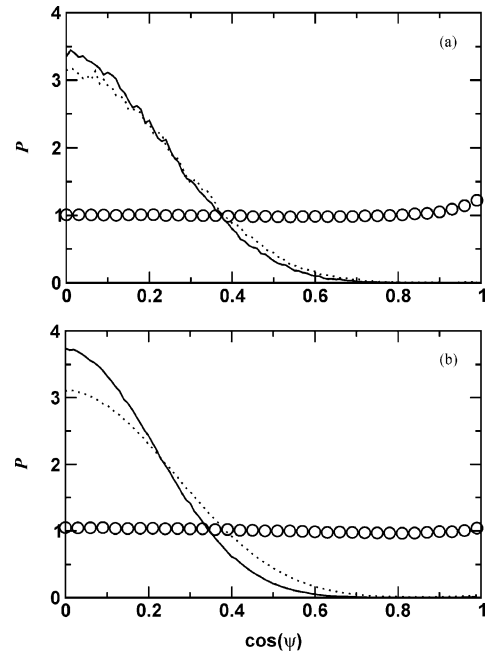

Figure 9. Distributions of the mutual orientation ψ for neighboring benzene molecules in the central region of the slab or the bulk liquid for the 6-site benzene model (top) and 9-site benzene model (bottom). Line styles and symbols as in Figure 7.

IV. Conclusions

Vapor−liquid and vapor−solid coexistence curves were determined for benzene applying Gibbs ensemble Monte Carlo simulations to a 6-site united-atom LJ model and a 9-site model with explicit quadrupolar interactions (six united-atom LJ sites and three out-of-plane partial charges). Although the 6-site model yields an adequate description of the vapor−liquid coexistence curve, it does not allow for a sufficient energetic gain for the benzene I structure and the triple point temperature is underestimated by about 130 K (or a factor of 2). Even at temperatures below its triple point, there is significant orientational disorder in the benzene I phase for the 6-site model. In contrast, the 9-site model yields slightly more accurate saturated vapor pressures and greatly improved sublimation pressures. The triple point temperature for the 9-site model is found to be about 25 K (or about 10%) below the experimental value. The benzene I phase for the 9-site model remains very ordered even as the temperature approaches the triple point temperature from below, thus showing the importance of the explicit quadrupolar interactions for stabilizing this phase with its T-shaped arrangement. However, the saturated solid density and correspondingly the liquid-to-solid density jump are slightly underestimated by the 9-site model. Furthermore, the heat of sublimation for the 9-site model is slightly too small.

Overall it appears that further improvements in the force field (e.g., an explicit representation of the hydrogens or a better representation of the charge distribution of benzene) would be required to yield an entirely satisfactory description of the complete phase diagram of benzene. The model might be further improved by explicitly including many-body polarization effects via fluctuating charges[54,55] or adding explicit three-body dispersive terms. However, it should be noted that excellent agreement for both the vapor−liquid and the vapor−solid coexistence line has been obtained recently for a fixed-charge model of carbon dioxide, thus nonpairwise-additive terms might not be as important as a better representation of the shape and charge distribution of benzene.

In closing, it should be noted here that the solid-slab Gibbs ensemble simulations become more difficult as the temperature is lowered (increasing concurrently the heat of sublimation and the solid density) and that this technique cannot be directly applied to determine solid−liquid melting lines. Thus, a promising approach would be to use the knowledge of the triple point properties (temperature, saturated vapor pressure, coexistence densities, and heat of fusion) as the starting point for Gibbs−Duhem integration[44] to obtain the melting line and to extend the sublimation line to lower temperatures.

Acknowledgment. We thank Collin Wick for many helpful discussions and Peter Monson for stimulating this research. Financial support from the National Science Foundation (CTS-0138393) is gratefully acknowledged. Part of the computer resources were provided by the Minnesota Supercomputing Institute.

References and Notes

(1) Evans, D. J.; Watts, R. O. *Mol. Phys.* **1976**, *32*, 93.
(2) Claessens, M.; Ferrario, M.; Ryckaert, J. P. *Mol. Phys.* **1983**, *50*, 217.
(3) Jorgensen, W. L.; Madura, J. D.; Swenson, C. J. *J. Am. Chem. Soc.* **1984**, *106*, 6638.
(4) Price, S. L.; Stone, A. J. *Mol. Phys.* **1984**, *51*, 569.
(5) Yashonath, S.; Price, S. L.; McDonald, I. R. *Mol. Phys.* **1988**, *64*, 361.
(6) Thiéry, M. M. *J. Chem. Phys.* **1988**, *89*, 4255.
(7) Jorgensen, W. L.; Severance, D. L. *J. Am. Chem. Soc.* **1990**, *112*, 4768.
(8) Khare, A. A.; Rutledge, G. C. *J. Chem. Phys.* **1999**, *110*, 3063.
(9) Errington, J. P.; Panagiotopoulos, A. Z. *J. Chem. Phys.* **1999**, *111*, 9731.
(10) Dang, L. X. *J. Chem. Phys.* **2000**, *113*, 266.
(11) Wick, C. D.; Martin, M. G.; Siepmann, J. I. *J. Phys. Chem. B* **2000**, *104*, 8008.
(12) Wick, C. D.; Siepmann, J. I.; Klotz, W. L.; Schure, M. R. *J. Chromatogr. A* **2002**, *954*, 181.
(13) Wyckoff, R. W. G. *Crystal Structures*, 2nd ed.; Interscience, New York, 1969; Vol. 6, p 1.
(14) Bacon, G. E.; Curry, N. A.; Wilson, S. A. *Proc. Roy. Soc. A* **1964**, *279*, 98.

(15) Piermarini, G. P.; Mighell, A. D.; Weir, S. E.; Block, S. *Science* **1969**, *165*, 1250.
(16) Dzyabchenko, A. V. *J. Struct. Chem.* **1984**, *25*, 416.
(17) Dzyabchenko, A. V. *J. Struct. Chem.* **1987**, *28*, 862.
(18) Dzyabchenko, A. V. *Sov. Phys. Crystallogr.* **1989**, *34*, 131.
(19) Shoda, T.; Yamahara, K.; Okazaki, K.; Williams, D. E. *J. Mol. Struct.*: *THEOCHEM* **1994**, *313*, 321.
(20) Shoda, T.; Yamahara, K.; Okazaki, K.; Williams, D. E. *J. Mol. Struct.*: *THEOCHEM* **1995**, *333*, 267.
(21) Gibson, K. D.; Sheraga, H. A. *J. Phys. Chem.* **1995**, *99*, 3765.
(22) Chaka, A. M.; Zaniewski, R.; Youngs, W.; Tessier, C.; Klopman, G. *Acta Crystallogr. B* **1996**, *52*, 165.
(23) van Eijck, B. P.; Spek, A. L.; Mooij, W. T. M.; Kroon, J. *Acta Crystallogr. B* **1998**, *54*, 291.
(24) Schroer, J. W.; Monson, P. A. *J. Chem. Phys.* **2000**, *112*, 8950.
(25) Schroer, J. W.; Monson, P. A. *J. Chem. Phys.* **2001**, *114*, 4124.
(26) Frenkel, D.; Ladd, A. J. C. *J. Chem. Phys.* **1984**, *81*, 3188.
(27) Polson, J. M.; Trizac, E.; Pronk, S.; Frenkel, D. *J. Chem. Phys.* **2000**, *112*, 5339.
(28) Vega, C. *Mol. Phys.* **1992**, *75*, 427.
(29) Lennard-Jones, J. E.; Devonshire, A. F. *Proc. R. Soc. London, Ser. A* **1937**, *163*, 53.
(30) Lennard-Jones, J. E. *Proc. Cambridge Philos. Soc.* **1931**, *27*, 469.
(31) Chen, B.; Siepmann, J. I. *J. Phys. Chem. B* **2001**, *105*, 9840.
(32) Panagiotopoulos, A. Z. *Mol. Phys.* **1987**, *61*, 813.
(33) Panagiotopoulos, A. Z.; Quirke, N.; Stapleton, M.; Tildesley, D. J. *Mol. Phys.* **1988**, *63*, 527.
(34) Howard, S. T.; Krygowski, T. M. *Can. J. Chem.* **1997**, *75*, 1174.
(35) Stolze, W. H.; Stolze, M.; Hübner, D.; Sutter, D. H. *Z. Naturforsch. A* **1982**, *37*, 1165.
(36) Yashonath, S.; Rao, C. N. R. *Mol. Phys.* **1985**, *54*, 245.
(37) Siepmann, J. I.; Frenkel, D. *Mol. Phys.* **1992**, *75*, 59.
(38) Mooij, G. C. A. M.; Frenkel, D. *Mol. Phys.* **1991**, *74*, 41.
(39) de Pablo, J. J.; Laso, M.; Suter, U. W. *J. Chem. Phys.* **1992**, *96*, 2395.
(40) Mackie, A. D.; Tavitian, B.; Boutin, A.; Fuchs, A. H. *Mol. Simul.* **1997**, *19*, 1.
(41) Vlugt, T. J. H.; Martin, M. G.; Smit, B.; Siepmann, J. I.; Krishna, R. *Mol. Phys.* **1998**, *94*, 727.
(42) Chen, B.; Siepmann, J. I. *J. Phys. Chem. B* **1999**, *103*, 4508.
(43) Chen, B.; Siepmann, J. I. *J. Phys. Chem. B* **2000**, *104*, 8725.
(44) Kofke, D. A. *Mol. Phys.* **1993**, *78*, 1331.
(45) Timmermans, J. *Physico-Chemical Constants of Pure Organic Compounds*; Elsevier: New York, 1950.
(46) Jackowski, A. W. *J. Chem. Thermodyn.* **1974**, *6*, 49.
(47) Castellan, G. W. *Physical Chemistry*, 3rd ed.; Benjamin/Cummings Publishing: Menlo Park, CA, 1983.
(48) Goodwin, R. D. *J. Phys. Chem. Ref. Data* **1988**, *17*, 1541.
(49) Agrawal, R.; Kofke, D. A. *Mol. Phys.* **1995**, *85* 43.
(50) Chen, B.; Karaborni, S.; Siepmann, J. I. Unpublished work.
(51) The internal energy, density, azimuthal angle ϕ, and mutual orientation ψ for the simulations using the slab setup were calculated by averaging only over the six innermost layers for solid phases or the central 30 Å for liquids.
(52) DeKruif, C. G.; van Ginkel, C. H. D. *J. Chem. Thermodyn.* **1977**, *9*, 725.
(53) Konicek, J. *Acta Chem. Scand.* **1973**, *27*, 1496.
(54) Rick, S. W.; Stuart, S. J.; Berne, B. J. *J. Chem. Phys.* **1994**, *101*, 6141.
(55) Chen, B.; Xing, J.; Siepmann, J. I. *J. Phys. Chem. B* **2000**, *104*, 2391.
(56) Majer, V.; Svoboda, V. *Enthalpies of Vaporization of Organic Compounds*: *A Critical Review and Data Compilation*; Blackwell Scientific Publications: Oxford, UK, 1985; p 300.
(57) Calado, J. C. R.; Dias, A. R.; Mina de Piedade, M. E.; Martinho Simoes, J. A. *Rev. Port. Quim.* **1980**, *22*, 53.